ChemComm

COMMUNICATION

View Article Online
View Journal | View Issue

Cite this: *Chem. Commun.*, 2022, **58**, 5538

Received 7th March 2022,
Accepted 7th April 2022

DOI: 10.1039/d2cc01341j

rsc.li/chemcomm

Construction of a dual-functional dumbbell probe-based fluorescent biosensor for cascade amplification detection of miRNAs in lung cancer cells and tissues†

Qian Zhang,‡[a] Yun Han,‡[a] Chen-chen Li,‡[b] Xiaoran Zou,[a] Fei Ma*[c] and Chun-yang Zhang *[a]

We develop a dual-functional dumbbell probe-based fluorescent biosensor for cascade amplification detection of miRNAs in lung cancer cells and tissues by integrating a primer exchange reaction (PER) with the CRISPR–Cas12a system. This biosensor can absolutely quantify the miR-486-5p expression in different lung cancer cells and distinguish non-small cell lung cancer (NSCLC) patients from healthy individuals, holding great potential in biomedical research and clinical diagnosis.

MicroRNAs (MiRNAs) are non-protein-coding single-stranded RNAs with the capability of inhibiting the translation of corresponding proteins by completely/incompletely matching with target messenger RNAs (mRNAs), and they regulate various cellular processes including differentiation and apoptosis.[1] The dysregulated expression of miRNAs may lead to tumorigenesis, tumor growth and metastasis by affecting several key processes (*e.g.*, promoting cancer cell proliferation, inhibiting apoptosis, and stimulating angiogenesis, migration, and invasion).[2] Consequently, miRNAs can act as important diagnostic biomarkers, prognostic indicators, and potential therapeutic targets. Lung cancer is the most lethal malignancy because it is mostly diagnosed at late stages, with non-small cell lung cancer (NSCLC) accounting for more than 80%.[3] Some miRNAs' expression levels change linearly over several consecutive stages from normal bronchial tissue to carcinoma. Quantitative miRNA expression can distinguish high-grade lesions from low-grade lesions, and can distinguish carcinoma *in situ* from invasive carcinoma as well.[4] Thus, the sensitive quantification of tumor-specific miRNAs is crucial for early NSCLC diagnosis.

Despite the progress in the development of miRNA detection methods,[5] simple and sensitive measurement of low abundance miRNAs in real samples (*e.g.*, tissue and serum) remains a challenge because of their inherent characteristics (*e.g.*, small size, intrinsic susceptibility and high sequence similarity).[6] qRT-PCR is frequently employed for miRNA assays, but it requires an accurate thermal cycler, trained personnel, and complex probe design.[7] Alternatively, loop-mediated isothermal amplification (LAMP),[8] exponential isothermal amplification (EXPAR)[9] and rolling circle amplification (RCA)[10] have been introduced for the construction of various fluorescent and electrochemical miRNA biosensors. However, they require the capability of switching between multiple temperatures at various procedures (for example, a total of three different temperatures are required for miRNA assays including 90 °C for denaturation, 16 °C for ligation, and 37 °C for RCA)[11] and the synthesis of the expensive circular template, and they suffer from the slow reaction kinetics of EXPAR induced by the increasing amounts of nicking enzyme[12] and time-consuming and laborious operation steps.[13] For practical applications, simple and rapid methods for sensitive detection of miRNAs are urgently demanded.

Recently, the primer exchange reaction (PER) has attracted more and more attention due to its compactness, simplicity, and ease of control.[14] Unlike polymerase/exonuclease/nickase (PEN) reaction networks that require sophisticated coordination among multiple enzymes and complex design of probes to achieve the cyclic generation of a specific sequence, the PER strategy can realize the cyclic synthesis of any sequence with the assistance of a hairpin, a short primer (7–9 nt) and a strand displacing polymerase, providing a robust platform for engineering molecular DNA circuits.[15] The powerful PER has been widely applied for biosensing of SARSCoV-2,[16] exosomal miRNA,[17] and survivin mRNA,[15] but the detection sensitivity is limited by its linear amplification nature. As revolutionary

[a] *College of Chemistry, Chemical Engineering and Materials Science, Shandong Normal University, Jinan 250014, China. E-mail: cyzhang@sdnu.edu.cn*
[b] *College of Chemistry and Molecular Engineering, Qingdao University of Science and Technology, Qingdao 266042, China*
[c] *School of Chemistry and Chemical Engineering, Southeast University, Nanjing, 211189, China. E-mail: fei@seu.edu.cn*

† Electronic supplementary information (ESI) available. See DOI: https://doi.org/10.1039/d2cc01341j

‡ These authors contributed equally.

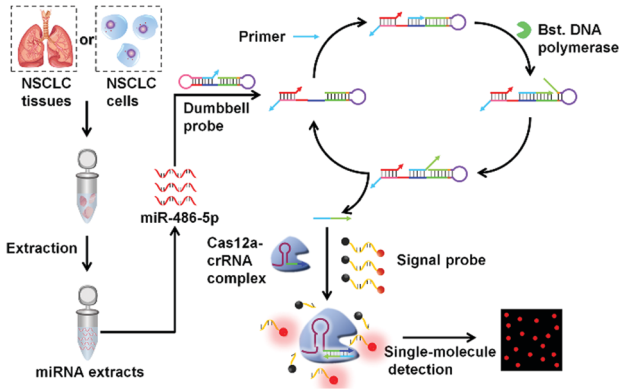

Scheme 1 Schematic illustration of the dual-functional dumbbell probe-based fluorescent biosensor for cascade amplification detection of miRNAs in lung cancer cells and tissues.

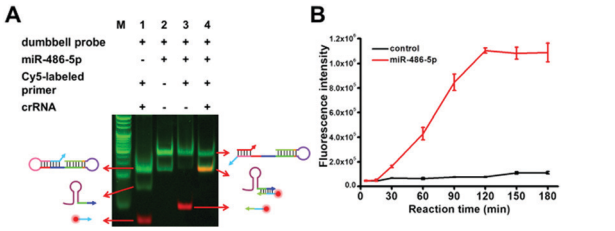

Fig. 1 (A) PAGE analysis of miR-486-5p-initiated PER reaction. Lane M, 20 bp DNA ladder; lane 1, 10 nM dumbbell probes + 100 nM Cy5-labeled primers + 80 nM crRNA; lane 2, 10 nM dumbbell probes + 10 nM miR-486-5p; lane 3, 10 nM dumbbell probes + 100 nM Cy5-labeled primers + 10 nM miR-486-5p; lane 4, 10 nM dumbbell probes + 100 nM Cy5-labeled primers + 10 nM miR-486-5p + 80 nM crRNA. (B) Dynamic changes of Cy5 fluorescence as a function of reaction time in response to the control (black line) and 10 nM miR-486-5p (red line).

gene-editing tools, the RNA-guided CRISPR–Cas systems have shown great promise for accurate nucleic acid diagnosis. Among all Cas nucleases, Cas12a performs collateral cleavage activity to indiscriminately cleave nearby single-stranded DNA (ssDNA).[18] Herein, we develop a dual-functional dumbbell probe-based fluorescent biosensor for cascade amplification detection of miRNAs in lung cancer cells and tissues (Scheme 1).

Scheme 1 shows the principle of microRNA detection. The miR-486-5p is used as a model target, and it is a tumor suppressor by regulating a protumorigenic gene to repress the metastasis and progression of NSCLC.[19] This assay involves a dumbbell probe, a short primer, and a signal probe. The dumbbell probe contains three functional domains including a miRNA binding domain (Scheme 1, pink color), a primer binding domain (Scheme 1, blue color), and a primer extending domain (Scheme 1, green color). Three consecutive G–C pairs (Scheme 1, orange color) located at a position close to the right loop region of the dumbbell probe serve as a stop codon for terminating polymerization. The addition of dATP, dTTP and dCTP (without dGTP) only can halt the extension of the primer when the first guanosine is encountered during polymerization. When miR-486-5p is present, it hybridizes with the binding domain of the dumbbell probe, resulting in the exposure of the complementary domain of the primer. The primer can bind with the unlocked dumbbell probe and be extended by Bst. large fragment DNA polymerase to generate an extended primer until the strand extension reaction is terminated at the stop site of the dumbbell probe. Subsequently, the extended region of the primer is competitively displaced by the complementary region of the template domain of the dumbbell probe through the random walk process of three-way branch migration, resulting in the dissociation of the extended primer from the dumbbell probe. The released dumbbell probe can bind other primers to induce the cyclical primer exchange reaction, generating abundant extended primers. The extended primer can function as an activator to hybridize with crRNA to activate the collateral cleavage activity of Cas12a protein, digesting the Cy5/BHQ2-labeled signal probes and recovering the Cy5 fluorescence signal. Target miRNA can be accurately quantified by monitoring the Cy5 fluorescence signal *via* single-molecule detection. In contrast, when miR-486-5p is absent, the primer binding domain of the dumbbell probe is blocked, and neither PER nor the activation of the collateral cleavage activity of Cas12a protein can occur. As a result, the signal probe remains intact and no Cy5 signal can be observed.

We calculated the standard free energy change (ΔG) and theoretical conversion efficiency (E) of the PER activation process and theoretically verified that even low-abundance target miR-486-5p can efficiently initiate PER (see ESI,† Fig. S1 and Tables S2, S3). We performed nondenaturing PAGE to verify the feasibility of this method (Fig. 1A). To clearly distinguish primers from other nucleic acid sequences, we modified the 5′ terminus of the primer with Cy5 for tracking in gel electrophoresis experiments. When the dumbbell probe, Cy5-labeled primer and crRNA coexist, the characteristic bands of the dumbbell probe, crRNA, and Cy5-labeled primer are observed (Fig. 1A, lane 1). When the dumbbell probe and miR-486-5p are present, a distinct band of miR-486-5p/dumbbell probe duplex appears, accompanied by the disappearance of the dumbbell probe band (Fig. 1A, lane 2), suggesting that the hybridization of the dumbbell probe with miR-486-5p enables the exposure of the complementary domain of the primer. When the dumbbell probe, miR-486-5p and Cy5-labeled primer coexist, a characteristic band corresponding to the extended Cy5-labeled primer is detected, suggesting that miR-486-5p induces the PER reaction (Fig. 1A, lane 3). When the dumbbell probe, miR-486-5p, Cy5-labeled primer and crRNA coexist, a yellow band with the colocalization of SYBR Gold and the Cy5 signal is detected (Fig. 1A, lane 4), suggesting that the products of Cy5-labeled primer extended by the PER reaction can hybridize with crRNA to obtain DNA/RNA hybrids. We further measured the dynamic curve of the reaction system (Fig. 1). In the presence of target miR-486-5p, the Cy5 signal increases with reaction time from 0 to 120 min and levels off at 120 min (Fig. 1B, red line), while the Cy5 signal remains unchanged in the control group without target (Fig. 1B, black line). The results clearly demonstrate that miR-486-5p can

initiate the PER-activated CRISPR–Cas12a-mediated dual signal amplification to recover Cy5 fluorescence.

Different from the ensemble fluorescence measurements, single-molecule detection is characterized by low sample consumption, high signal-to-noise ratio, and high sensitivity.[20] We detected the target signal using total internal reflection fluorescence (TIRF) microscope-based single-molecule imaging (ESI,† Fig. S2). When miR-486-5p is absent, no Cy5 spot is detected (Fig. 2A), indicating no occurrence of CRISPR–Cas12a-assisted recycling cleavage reaction. On the contrary, when miR-486-5p is present, distinct Cy5 spots are generated (Fig. 2B), suggesting that target miR-486-5p can induce the PER reaction and subsequently initiate the CRISPR–Cas12a-assisted recycling cleavage reaction to generate Cy5 fluorescence signals. Notably, the Cy5 fluorescent spots exhibit irreversible one-step photobleaching (Fig. 2C), suggesting a single-molecule event for each observed Cy5 spot. These results demonstrate the feasibility of this biosensor to accurately quantify miR-486-5p at the single-molecule level.

The sensitivity of this biosensor was investigated under the optimized conditions (see ESI,† Fig. S3). Cy5 counts improve when the miR-486-5p concentration increases from 1 fM to 10 nM (Fig. 3A), and the Cy5 counts (N) display linear dependence upon the miR-486-5p concentration (C) in logarithmic scale (Fig. 3B), with the equation being $N = 5872.89 + 360.57 \lg C$ ($R^2 = 0.998$). The detection limit is determined to be 0.45 fM (9 zmol). Notably, the assay performance of this biosensor is superior/comparable to those of reported sensing strategies in terms of the number of required enzymes and temperatures, the involved steps, assay time, and detection limit (see ESI,† Table S4).[10,21]

We selected single-base mismatched miR-486-5p (miR-486-5p M1), double-base mismatched miR-486-5p (miR-486-5p M2), three base-mismatched miR-486-5p (miR-486-5p M3), miR-4529-3p, and an irrelevant miRNA (let-7a) as the interference sequences. A low Cy5 signal is generated by let-7a, miR-4529-3p, miR-486-5p M3, miR-486-5p M2, miR-486-5p M1, and the control without any miRNA, respectively (Fig. 3C). However, a high Cy5 signal is generated by target miR-486-5p, which is 15.14, 14.75, 13.80, 12.08, 8.84, and 6.94-fold higher than that of control group, let-7a, miR-4529-3p, miR-486-5p M3, miR-486-5p M2 and miR-486-5p M1, respectively (Fig. 3C), suggesting that this biosensor can even distinguish the single-base mismatch.

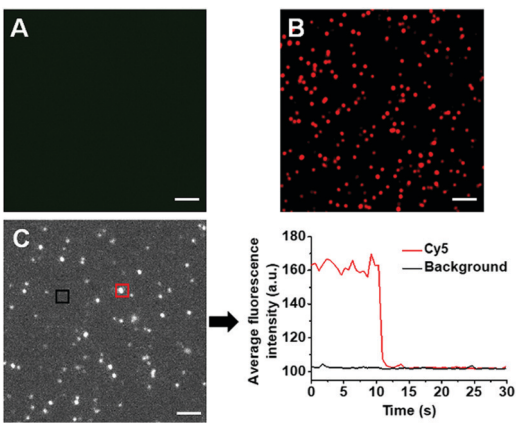

Fig. 2 (A and B) Representative fluorescence images of Cy5 in the absence (A) and presence (B) of target miR-486-5p (10 nM). (C) Photobleaching trajectory of individual Cy5 spots over time. The left panel shows the single-molecule fluorescence image prior to photobleaching. The scale bar is 2.5 μm.

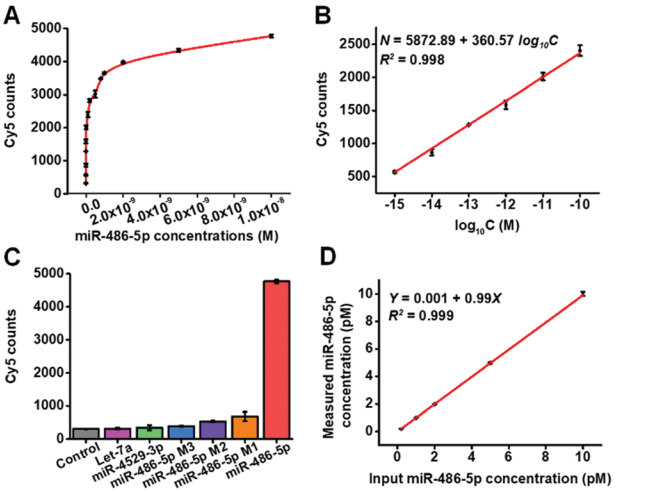

Fig. 3 (A) Plots of Cy5 counts *versus* various concentrations of target miR-486-5p. (B) Linear dependence of Cy5 counts upon the miR-486-5p concentration in logarithmic scale. (C) Measurement of Cy5 fluorescence signal generated by the reaction buffer (control, gray column), 10 nM miR-486-5p (red column), 10 nM miR-4529-3p (green column), 10 nM let-7a (magenta column), 10 nM miR-486-5p M3 (blue column), 10 nM miR-486-5p M2 (violet column), and 10 nM miR-486-5p M1 (orange column), respectively. (D) Measured miR-486-5p concentration exhibits good correlation with the actual input miR-486-5p concentration.

To demonstrate the anti-interference capability of this biosensor, we performed a recovery study by spiking various concentrations of miR-486-5p (0.2–10 pM) in 10% normal human serum. The recovery ratio of 98.58–100.6% with a relative standard deviation (RSD) of 0.3–1.5% is obtained (see ESI,† Table S5). Notably, the measured miR-486-5p concentration (Y) is linearly proportional to the actual input miR-486-5p concentration (X) (Fig. 3D), with the correlation equation being $Y = 0.001 + 0.99X$ ($R^2 = 0.999$), suggesting the reliability of this biosensor for complex biological sample analysis.

We further measured the miR-486-5p expression in NSCLC cell lines including H460 cells, H292 cells, H358 cells, A549 cells, and H1975 cells. The miR-486-5p concentration (Fig. 4A, red columns) was calculated according to the linear fitting equation (Fig. 3B). Our results indicate that the miR-486-5p expression level in human NSCLC cell lines decreases in the order of H358 cells > H292 cells > A549 cells > H1975 cells > H460 cells (Fig. 4A, red columns), which is consistent with the previous literature.[3] The miR-486-5p expression level in five types of NSCLC cell lines was further quantified by gold standard qRT-PCR (see ESI,† Fig. S4), and the obtained results (Fig. 4A, green columns) are consistent with those obtained by this biosensor (Fig. 4A, red columns).

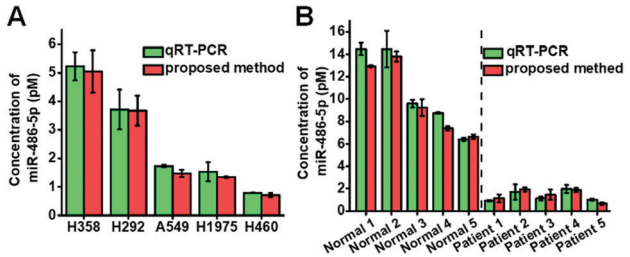

Fig. 4 (A) Measurement of the miR-486-5p expression in total RNA from various types of human NSCLC cell lines by this biosensor (red columns) and qRT-PCR (green columns). (B) Quantitation analysis of the miR-486-5p expression level in lung tissues of healthy individuals and NSCLC patients by qRT-PCR (green columns) and this biosensor (red columns).

To assess the potential of this biosensor in clinic diagnosis, we monitored the miR-486-5p expression in human tissue samples from 5 diagnosed NSCLC patients and 5 healthy individuals. The measured miR-486-5p concentration in NSCLC tissues is remarkably lower than that in normal lung tissues (*t*-test, $P = 0.00036 < 0.001$) (Fig. 4B, red columns), with a median concentration of 9.63 pM for normal lung tissues and 1.92 pM for NSCLC tissues (see ESI,† Table S6), suggesting downregulation of miR-486-5p expression in NSCLC tissues.[3] Meanwhile, the miR-486-5p expression in tissues is quantified by the qRT-PCR method, and the obtained results (Fig. 4B, green columns) are consistent with those obtained by this biosensor (Fig. 4B, red columns).

In conclusion, we have developed a dual-functional dumbbell probe-based fluorescent biosensor for cascade amplification detection of miRNAs in lung cancer cells and tissues. This biosensor possesses unique characteristics: (1) the designed dumbbell probe integrates target miRNA recognition with PER amplification in one probe, endowing this assay with an extremely low background due to the perfect folding of the dumbbell probe; (2) the integration of single-molecule detection with PER-activated CRISPR–Cas12a-mediated dual signal amplification endows this biosensor with improved sensitivity; (3) the whole amplification reaction can be carried out at a constant temperature, eliminating the need for tedious switching between multiple temperatures; (4) this assay can be performed in a one-pot reaction by simply mixing the commercially available materials, without the requirement of laborious separation/washing steps. This biosensor can sensitively detect miRNA with a detection limit of 0.45 fM (9 zmol) and distinguish single-base mismatches as well. Moreover, it can absolutely quantify the miR-486-5p expression in different types of lung cancer cells and even discriminate healthy individuals from NSCLC patients. Importantly, this biosensor can be easily reconfigured to monitor different target miRNAs by simply altering the corresponding recognition sequences, with great promise in the early diagnosis of diseases.

This work was supported by the National Natural Science Foundation of China (Grant No. 21735003) and the Award for Team Leader Program of Taishan Scholars of Shandong Province, China.

Conflicts of interest

There are no conflicts to declare.

Notes and references

1 J. C. Carrington and V. Ambros, *Science*, 2003, **301**, 336–338.
2 J. Lu, G. Getz, E. A. Miska, E. Alvarez-Saavedra, J. Lamb, D. Peck, A. Sweet-Cordero, B. L. Ebert, R. H. Mak, A. A. Ferrando, J. R. Downing, T. Jacks, H. R. Horvitz and T. R. Golub, *Nature*, 2005, **435**, 834–838.
3 J. Wang, X. Tian, R. Han, X. Zhang, X. Wang, H. Shen, L. Xue, Y. Liu, X. Yan, J. Shen, K. Mannoor, J. Deepak, J. M. Donahue, S. A. Stass, L. Xing and F. Jiang, *Oncogene*, 2014, **33**, 1181–1189.
4 S. L. Yu, H. Y. Chen, G. C. Chang, C. Y. Chen, H. W. Chen, S. Singh, C. L. Cheng, C. J. Yu, Y. C. Lee, H. S. Chen, T. J. Su, C. C. Chiang, H. N. Li, Q. S. Hong, H. Y. Su, C. C. Chen, W. J. Chen, C. C. Liu, W. K. Chan, W. J. Chen, K. C. Li, J. J. Chen and P. C. Yang, *Cancer Cell*, 2008, **13**, 48–57.
5 H. Dong, J. Lei, L. Ding, Y. Wen, H. Ju and X. Zhang, *Chem. Rev.*, 2013, **113**, 6207–6233.
6 C. Xue, M. Luo, L. Wang, C. Li, S. Hu, X. Yu, P. Yuan and Z. S. Wu, *Anal. Chem.*, 2021, **93**, 9869–9877.
7 C. C. Pritchard, H. H. Cheng and M. Tewari, *Nat. Rev. Genet.*, 2012, **13**, 358–369.
8 Y. Sun, H. Tian, C. Liu, Y. Sun and Z. Li, *Chem. Commun.*, 2017, **53**, 11040–11043.
9 X. Wang, H. Wang, C. Liu, H. Wang and Z. Li, *Chem. Commun.*, 2017, **53**, 1124–1127.
10 W. Tian, X. Liu, G. Wang and C. Liu, *Chem. Commun.*, 2020, **56**, 13445–13448.
11 P. Qin, L. Yao, J. Xu, G. Liu and W. Chen, *Chem. Commun.*, 2019, **55**, 14367–14370.
12 M. S. Reid, R. E. Paliwoda, H. Zhang and X. C. Le, *Anal. Chem.*, 2018, **90**, 11033–11039.
13 F. Ma, W. J. Liu, Q. Zhang and C. Y. Zhang, *Chem. Commun.*, 2017, **53**, 10596–10599.
14 J. Y. Kishi, T. E. Schaus, N. Gopalkrishnan, F. Xuan and P. Yin, *Nat. Chem.*, 2018, **10**, 155–164.
15 J. Zhang, M. He, C. Nie, M. He, Q. Pan, C. Liu, Y. Hu, T. Chen and X. Chu, *Chem. Sci.*, 2020, **11**, 7092–7101.
16 (*a*) Y. Dai, W. Xu, R. A. Somoza, J. F. Welter, A. I. Caplan and C. C. Liu, *Angew. Chem., Int. Ed.*, 2020, **59**, 20545–20551; (*b*) D. Li, C. Duan, W. Cheng, Y. Gong, Y. Yao, X. Wang, Z. Wang and Y. Xiang, *Chem. Commun.*, 2022, **58**, 4484–4487.
17 X. Li, X. Li, D. Li, M. Zhao, H. Wu, B. Shen, P. Liu and S. Ding, *Biosens. Bioelectron.*, 2020, **168**, 112554.
18 J. S. Chen, E. Ma, L. B. Harrington, M. Da Costa, X. Tian, J. M. Palefsky and J. A. Doudna, *Science*, 2018, **360**, 436–439.
19 M. Boeri, C. Verri, D. Conte, L. Roz, P. Modena, F. Facchinetti, E. Calabro, C. M. Croce, U. Pastorino and G. Sozzi, *Proc. Natl. Acad. Sci. U. S. A.*, 2011, **108**, 3713–3718.
20 Q. Zhang, Y. Wu, Q. Xu, F. Ma and C. Y. Zhang, *Biosens. Bioelectron.*, 2021, **171**, 112712.
21 (*a*) G. Wang, W. Tian, X. Liu, W. Ren and C. Liu, *Anal. Chem.*, 2020, **92**, 6702–6708; (*b*) X. Tang, R. Deng, Y. Sun, X. Ren, M. Zhou and J. Li, *Anal. Chem.*, 2018, **90**, 10001–10008; (*c*) G. Zhang, L. Zhang, J. Tong, X. Zhao and J. Ren, *Microchem. J.*, 2020, **158**, 105239; (*d*) H. H. Sun, F. He, T. Wang, B. C. Yin and B. C. Ye, *Analyst*, 2020, **145**, 5547–5552; (*e*) J. Hu, M. H. Liu and C. Y. Zhang, *Chem. Sci.*, 2018, **9**, 4258–4267.